Effects of a Capacitively-Coupled Ground Plane on Nanohoneycomb Thin Films near the Insulator-Superconductor Transition

Alexander Levine

Advisor: James Valles, Jr.

May 2016

1 Introduction

Numerous materials exhibit superconductivity, a state of zero measurable resistivity and perfect diamagnetism, when cooled below a superconducting transition temperature T_c. In conventional superconductors, this transition is due to the formation of electron pairs known as Cooper pairs, which condense into a coherent macroscopic wave function, allowing them to carry charge through the material without scattering.

In thin films, T_c is reduced as thickness decreases: below a certain thickness, superconductivity becomes impossible, and resistance increases as temperature approaches zero. This creates a thickness-tuned Insulator-Superconductor transition (IST). In uniform films, this transition is thought to be due to the destruction of Cooper pairs due to electron localization. However, in films with thickness variations, localized Cooper pairs are believed to be present in the insulating state, leading to reentrant behavior in the plot of resistance versus

temperature (Figure 1) as, with decreasing temperature, the resistance first drops due to Cooper pair formation, and then increases due to localization of Cooper pairs.[1]

Figure 1: Thickness tuned IST for (A.) uniform amorphous film, (B.) undulating NHC film. Taken from [1].

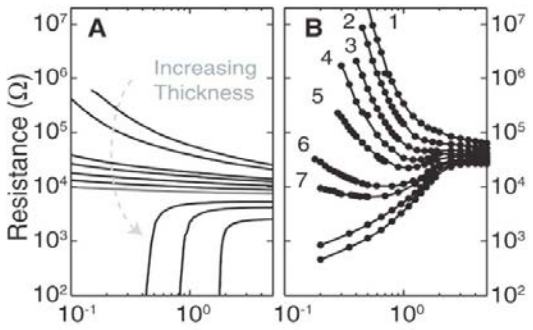

One way that a thin film with thickness variations can be made is by condensing metals onto anodized aluminum oxide substrates. Under certain electrochemical conditions, a porous oxide layer can be formed on the surface of aluminum. The pores can be made to form at regular intervals, to create a hexagonal lattice. By using this porous anodized aluminum oxide (AAO) as a substrate for quench condensation of a metal film, one can create films with this regular hexagonal geometry: these are known as nanohoneycomb (NHC) films.

Previous work by the Valles lab [1,2, 10] has shown that these films have regular thickness variations due to the geometry of the AAO substrate. Furthermore, on the insulating side of the thickness-tuned IST, these thickness variations create islands of the film thick enough to superconduct as uniform films at a given temperature, which are separated from each other by regions expected to have finite resistance. These islands occur at the nodal regions between holes; see Figure 2. Measurements of resistance as a function of temperature on the insulating side of the IST show thermally activated conductivity, and

measurements of resistance as a function of applied magnetic field show oscillatory behavior. These observations are similar to those taken in 2D Josephson junction arrays (JJAs).

Figure 2: AFM image of NHC film. Scale shown on the right image relative surface height in nanometers. White bar is 100 nm. Taken from [2].

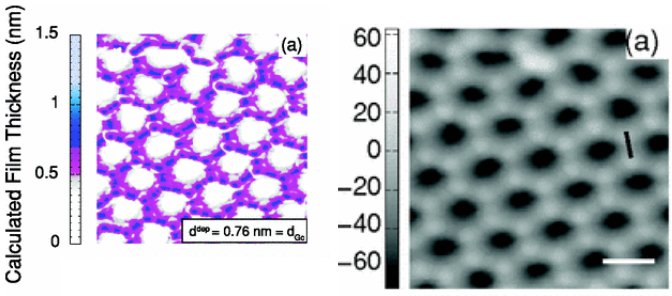

Figure 3: Schematic of cross-section of substrate and film. Taken from [10].

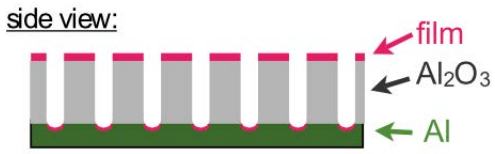

This thesis will examine the possible effects of capacitive coupling between the NHC film and the aluminum ground plane on which the AAO is grown on the film's behavior near the insulator-superconductor transition.

2 Charging Energy in the Josephson Junction Array Model

Josephson junction arrays are lithographically manufactured arrays of superconducting grains, separated by small insulating junctions. Cooper pairs can tunnel across these junctions via the Josephson effect; the Hamiltonian for the

array (in the absence of magnetic field) is given by [3]:

$$H = \frac{1}{2}Q^T C^{-1} Q - E_J \sum_{<i,j>} cos(\phi_i - \phi_j) \tag{1}$$

Where Q is a vector of the charges Q_i on each individual superconducting grain, C is a matrix specifying the capacitances between each grain as well as the self-capacitance of each grain, ϕ represents the superconducting phase parameter of each individual grain, $\sum_{<i,j>}$ denotes a sum over adjacent pairs, and E_J is the Josephson energy of each junction, assumed here to be uniform. Note that Q_i and ϕ_i are conjugate variables: $[\phi_i, Q_i] = 1$ for Q_i measured in units of 2e (Cooper pair charges.)

The first term of this Hamiltonian represents the total energy of the charge distribution due to electrostatic effects: consider the vector V, such that V_i is the electrostatic potential at grain i. Then we have, for the energy required to assemble the charges Q, $H_{electrostatic} = \frac{1}{2}V^T Q$. We will define the matrix C in such a way that $Q = CV$ holds as a vector equation: $Q_i = \sum_j C_{ij} V_j$.

To understand the elements that make up this matrix, first suppose that islands i and j have an interface with capacitance C_1. Then we expect that the charge on grain i at this interface is given by $Q_{i,interface\ with\ j} = C_1 \cdot (V_i - V_j)$. Then $C_{i,j} = -C_1$, and the interface contributes $+C_1$ to $C_{i,i}$. We can see by the symmetry of the problem that $C_{j,i}$ must also be $-C_1$; in fact, C must be a symmetric matrix. Finally, suppose that the grain i has a capacitance to ground ($V = 0$) of C_0. Then, disregarding charges at interfaces (which are neutralized at the other side of the interface), if i has a charge $Q_{i,bulk}$, then $Q_{i,bulk} = C_0 \cdot V_i$. So the capacitance to ground contributes $+C_0$ to $C_{i,i}$. Now, given $Q = CV$, we therefore have $V^T = Q^T (C^T)^{-1} = Q^T C^{-1}$, so $H_{electrostatic} = \frac{1}{2}Q^T C^{-1} Q$, as originally stated in equation (1).

Figure 4: Schematic of capacitances in a JJA. Each black circle represents a grain. Josephson junctions are present between adjacent grains, along with the labeled capacitance C_1. Two adjacent grains i and j are labelled as well. Taken, with modifications, from [9].

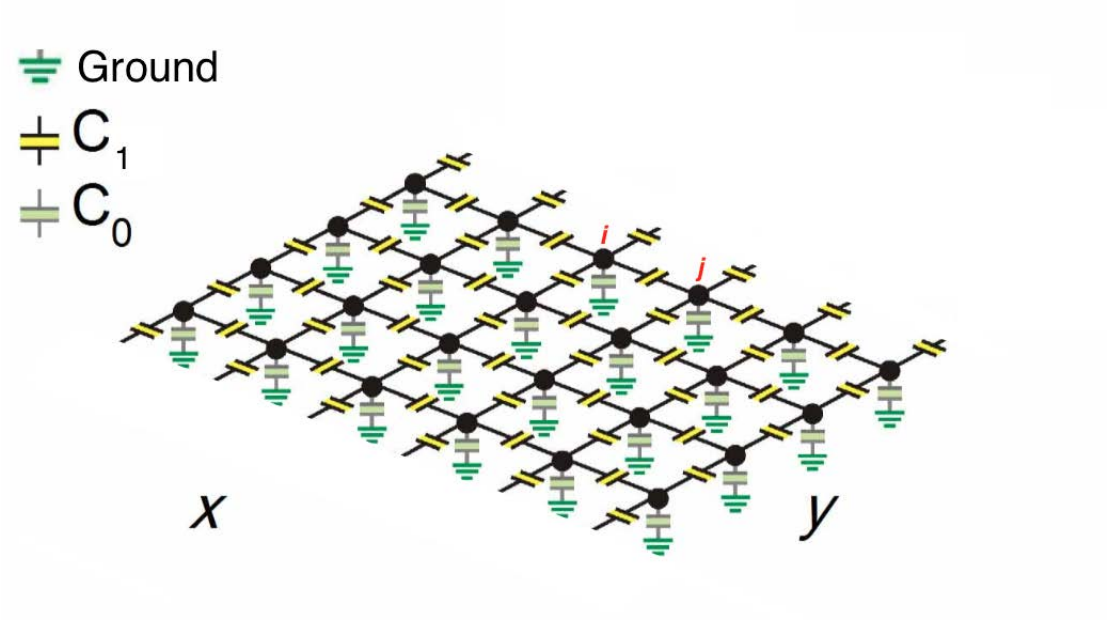

We can define a charging energy,

$$E_C = \frac{e^2}{2}(C^{-1})_{i,i} \tag{2}$$

representing the energy required for an isolated "free" electron to exist on a grain.(The energy required for a free Cooper pair is four times this value.) This can be derived from the the electrostatic term in the Hamiltonian (equation (1)) by simply setting Q to zero at all points except some i, and to e at Q_i. The smaller this value, the more easily individual grains can become charged: in other words, the smaller E_C is, the easier it is for free charge carriers to exist. In particular, in two-dimensional Josephson junction arrays, we expect the array to be insulating for $E_C >> E_J$, and conducting for $E_C << E_J$.[5]

This can be understood as simply a comparison of E_C to the only other energy scale present in the Hamiltonian.

In the insulating phase, both experimental and theoretical results [8] have given evidence for activated conductivity (that is, conductivity proportional to $e^{\frac{-T_0}{T}}$, where T is temperature), with activation energy T_0 on the order of E_C. This can be understood from the perspective of Boltzmann statistics, with the conductivity being related to the fraction of charge carriers able to obtain energy $> E_C$.

The value of $(C^{-1})_{ii}$, and therefore E_C, depends on the electrostatic configuration of the superconducting grains. In a commonly-accepted [4,5,9] model of JJA's, C is constructed from an inter-grain capacitance C_1 that exists only between immediately-adjacent grains, and a capacitance to ground C_0 on each grain. A schematic of this configuration is shown in Figure 4. As noted in [4], many treatments of JJAs simplify this model by neglecting either C_1 or C_0, depending upon the geometric properties of the array. In these cases, E_C reduces to $\frac{e^2}{2C_0}$ and $\frac{e^2}{2C_1}$, respectively.

in general, $(C^{-1})_{ii}$ and therefore E_C can be decreased by increasing either C_0 or C_1. Kopeć and José [4] give a general closed-form expression for $(C^{-1})_{ii}$ in infinite square JJA's using the nearest-neighbor model, in terms of C_0 and C_1:

$$(C^{-1})_{ii} = \frac{2}{\pi(C_0 + 4C_1)} K(\frac{4C_1}{(C_0 + 4C_1)}) \tag{3}$$

Where K is the elliptic integral of the first kind.
(They also derive expressions for hexagonal and triangular geometries.)

One should note that, in the limit $C_1 >> C_0$, this model of an infinite lattice is not applicable to finite systems: in this model, the potential on nearby grains due to a single isolated charge scales with distance from that charge as

$K_0(\frac{d}{\lambda})$, where d is distance number of grains, $\lambda = \sqrt{\frac{C_1}{C_0}}$, and K_0 is the modified Bessel function of the second kind. [9] For large C_1, λ can easily be larger than the size of the array: then the potential can not possibly be distributed according to this formula, so the model cannot be valid. In their simulations of activation energy in the case of hopping conductivity between grains, Ortuño et al. [9] derive an expression of $E_{ac} = E_0 ln(min\{L, \lambda\})$, where L is the side length of the array. To show the direct effect of finite array size on $(C^{-1})_{ii}$, see Figure 5, where we plot Kopeć and José's formula along with direct calculation of $(C^{-1})_{ii}$ in the nearest-neighbor model for various grid sizes.

Figure 5: Deviation in the predicted charging energy with finite array size where $C_1 >> C_0$. The light blue line is given by the formula for infinite grid size from Kopeć and José, and the dark blue, green, and red lines represent $(C^{-1})_{ii}$, taken as a mean over all grains in the array, in arrays with side length $L = 30, 50$, and 70, respectively: this is proportional to the mean charging energy of all grains. We see that the charging energy deviates significantly in the finitely-sized arrays from the charging energy in an infinitely-sized array as λ approaches L.

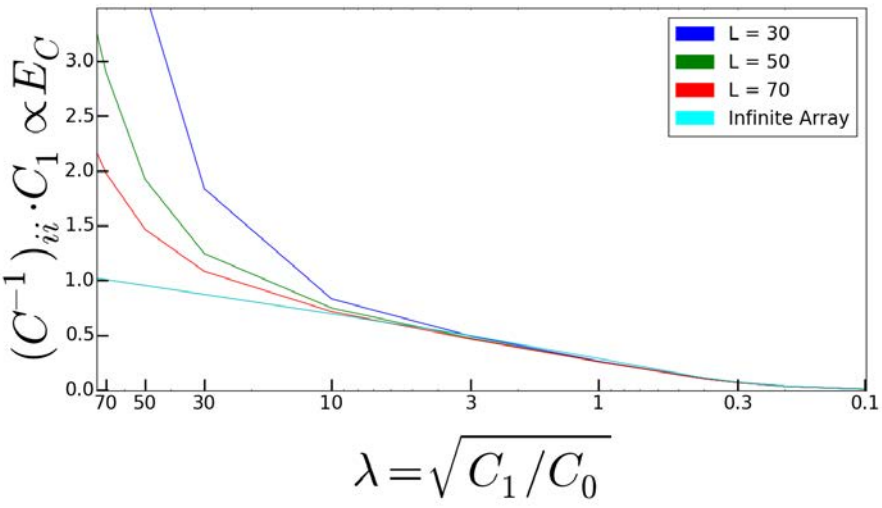

3 Possible Charging Effects in NHC Films

As stated in the introduction, NHC films have been shown, through microscopy techniques, to contain, in the insulating regime near the IST, regions thick enough to superconduct separated at regular intervals by thinner junctions.[2,10] The activated conductivity in the insulating phase, along with measurements of resistance as a function of applied magnetic field which show oscillatory behavior, have led to the hypothesis that, in the insulating phase, the NHC films behave like Josephson junction arrays in the domain where $E_C > E_J$. [1,2,10] However, in this previous work by the Valles lab, using capacitance values predicted based on AFM measurements of film geometry to determine island sizes and separation has given predicted values of E_C several orders of magnitude greater than the measured activation energy. [1] In particular, the charging energy calculated based on the geometric self-capacitance of a spherical island the size of the nodal regions between holes in the honeycomb lattice $\approx 50nm$ was at least two orders of magnitude larger than the measured activation energy. One proposed explanation [1,10] is that the effective superconducting island size is much larger than the geometric island size of the nodal regions, covering a larger area of the film: this increases both the island self-capacitances and the capacitances between adjacent islands by making each island larger, driving down E_C. In the case of these massive islands, the aluminum substrate layer underneath the $\approx 1\mu m$ AAO layer on which the film is grown may act as a capacitively-coupled ground plane. The larger-area effective islands may have significant mutual capacitances with the ground plane, contributing to C_0 in addition to the self-capacitances of the islands. This effect would also reduce E_C and therefore the predicted activation energy. Note that island size and capacitance to the ground plane should scale proportionately to island area, while inter-island capacitance should scale with the length of the interfaces: this means that in

the case of larger islands, C_0 has a greater role in determining E_C compared to the case of smaller islands. This means that if large effective superconducting islands are in fact being formed, the capacitance to the ground plane may become a variable in determining the charging energy. The following section presents a computational result relevant to understanding this scaling.

Finally, previous experimental work by Astrakharchik and Adkins [6] on uniform films has shown an increase in T_C at a given film thickness due to a proximal conducting ground plane. This is believed to be due to a screening of Coulomb interactions between electrons by the formation of image charges in the conductor. This screening reduces the net electrostatic interactions between electrons, preventing the destruction of Cooper pairs due to electron localization. Astrakharchik and Adkins cite Al'tshuler et al.[15], who analyse this screening in 2D normal metals with a proximal ground plane separated by a dielectric, and give a predicted correction to the electron-electron interaction as a function of the thickness and dielectric constant of the dielectric layer. By increasing T_C at each thickness, this effect may also come into play in our islanding model, by increasing the effective island sizes at a given temperature, and thus driving down E_C.

Clearly, then, the interaction between the film and the ground plane may be a parameter in the behavior of the films. Previous work by the Valles lab has not controlled for AAO thickness or capacitance across this layer: in section 5, we will begin to attempt to design procedures for measurement of these variables.

4 Numerical Simulations of $(C^{-1})_{ii}$ in Percolating Systems

In the previous section, it was discussed that large effective island sizes may lead to diminished E_C in NHC films.[1] Additionally, it is theorized that the thickness-tuned transition to superconductivity in NHC films is due to the thin junctions between islands reaching their uniform-film IST's: this creates a coalescence of islands, which become very large at the IST. [2, 10] We can model the formation of large effective islands as a percolative process, with the probability of any microscopic junction becoming conductive fixed independently of nearby junctions. Then the probability of two large effective islands merging is proportional to the number of weak links in their interface.

Earlier, it was stated that larger islands lead to lower $(C^{-1})_{ii}$, and therefore E_C, by increasing the scale of C_1 linearly with island diameter, and the scale of C_0 quadratically with island diameter. However, in Figure 6, we present simulations that show that, starting with a square lattice, networks produced by percolation have lower $(C^{-1})_{ii}$ than equivalent networks produced by simply scaling up the island size. In this figure, the value of $(C^{-1})_{ii}$ shown is the area-weighted median value among the islands in the network. Because these percolative networks have lower charging energies than square arrays with the same average island size, we might expect that the percolative system might transition to conductivity at a smaller average island size than would be conductive in uniform square arrays. Because C_0 becomes relatively more important as the island areas become larger, this further underscores the possible importance of the interaction with the ground plane in the NHC system.

Figure 6: Blue: $(C^{-1})_{ii}$ (proportional to the charging energy) versus number of grains, N, per side, in square arrays. Initially, $C_1 = 1, C_0 = .01$, and $N = 50$. For smaller N, the sum of C_0 over the entire array was held constant, reflecting the constant total area, and thus capacitance to ground, of all of the grains combined, and C_1 was scaled as $\frac{1}{N}$, reflecting the increasing diameter of the islands. In other words, this line represents the change in charging energy as island size increases, if the islands increase in size isometrically. The charging energy shown is the median charging energy over all grains.
Red: Each of the 10 lines represents a random percolation simulation, where, starting with a 50×50 grid with $C_1 = 1, C_0 = .01$, adjacent grains were randomly merged, with probability proportional to the capacitance between the two grains (i.e., the number of microscopic links in the interface between them). The capacitances to ground of the two grains were then added, as were the capacitances to any adjacent grains. The x axis is the square root of the number of remaining grains, so that the total grain number, and thus the average grain area, matches the line for the square array. The lines terminate when there exists a single grain bordering both the left and the right edge of the array: at this point, there is effectively a single grain involved in conduction. The values shown are the median charging energies, weighted by grain area: this should approximately be the minimum over all paths across the film of the maximum charging energy on that path, which should be the limiting charging energy for conduction.

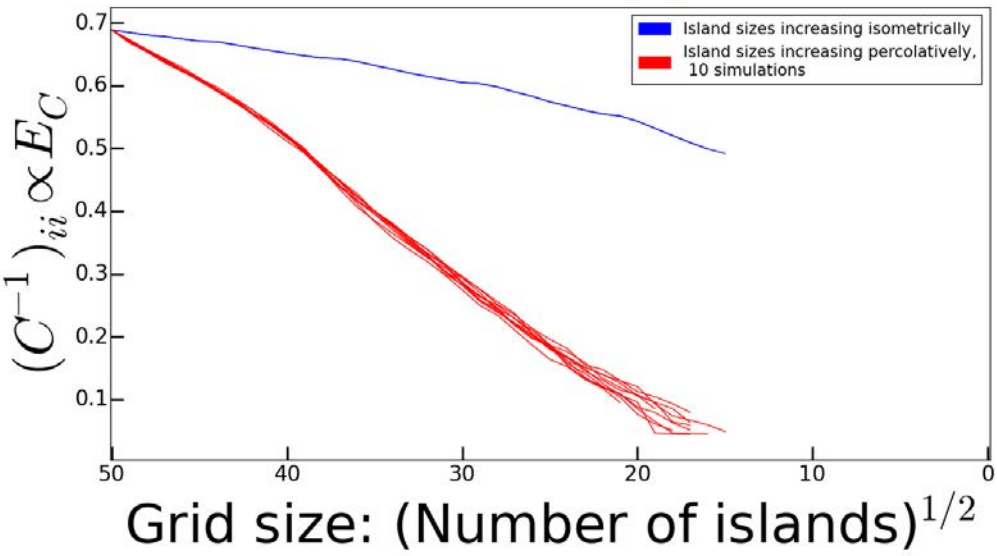

5 Geometric Parameters of AAO Relevant to Screening

In the case of large islands spanning the area of many holes, the capacitance between each island and the ground plane is the dominating term in C_0. Because many of the metal NHC films under study are conductive at room temperature, we can directly measure the capacitance of the entire film to the ground plane. By dividing by the area of the film, we can then determine the capacitance per unit area between the islands and the ground plane, which then determines C_0 per unit island area.

Other measurable parameters of the oxide layer may also have an impact on E_C. In particular, as mentioned in section 3, in regions of the film in the insulating phase prior to the formation of localized Cooper pairs, just as in the uniform films studied in [6], screening of the electrostatic force in individual electron-electron interactions by image charges in the ground plane may be relevant in lowering the energy required to form Cooper pairs, thereby raising T_C. By allowing larger islands to form, this could then lower E_C. The parameters relevant to this process proposed in [12] were the thickness of the dielectric layer d along with dielectric constant of this layer. Note that this d cannot be immediately calculated from the measured capacitance per unit area of the film and the reference dielectric constant of aluminum oxide ($\epsilon_{r,Al_2O_3} = 10.2$ [11]): the film area, measured macroscopically, includes the area of the holes, which are not covered by the film itself, and have a lower dielectric constant than the aluminum oxide surrounding them. Then further measurements are needed to determine d.

In section 6, we will present computational results to relate the measured capacitance per unit area to the substrate thickness and the hole diameter and

spacing. In section 7, we will present procedures developed to measure the total capacitance per unit area of a film. In section 8, we will present attempts at developing efficient techniques for measuring d.

6 Modelling the electrostatics of an NHC patterned film condensed on a porous aluminum oxide substrate with an aluminum underlayer

This section attempts to answer the question of how the presence of holes affects the measured dielectric constant of the AAO layer in our film systems. Let us model the AAO layer as an infinite plane of dielectric material, of thickness d and relative dielectric constant $\epsilon_{Al_2O_3}$, sandwiched between two capacitor plates. There are regularly-spaced holes in both the dielectric and in the top capacitor plate (i.e., the film), in a hexagonal lattice. The dielectric constant within the holes is $\epsilon_{hole} \approx \epsilon_0$. Naively, two possible approximations seem applicable. The first is to treat the system as a simple parallel plate capacitor, with the dielectric constant of the area-weighted average of the two values, ignoring the fact that the top capacitor plate also has holes:

$$C_{AWA} = \frac{A_{Al_2O_3}\epsilon_{Al_2O_3} + A_{hole}\epsilon_{hole}}{d} \tag{4}$$

The other naive approximation is to neglect the area in the holes entirely:

$$C_{NH} = \frac{A_{Al_2O_3}\epsilon_{Al_2O_3}}{d} \tag{5}$$

In order to determine which approximation is more accurate, a computer model of the electrostatic configuration was made, and the potential was cal-

culated everywhere for oppositely charged plates using the Finite Differences method, handling the dielectric boundaries using an offset grid as described in [12]. The infinite extent of the lattice was modeled using reflective boundary conditions. $\epsilon_{Al_2O_3}$ was taken as 10, and ϵ_{hole} was taken as 1. An example run, with hole radius $\frac{3}{7}$ of the maximum possible radius before holes overlap and $d = \frac{1}{2}$ times the distance between centers of holes is shown in Figure 7. Figure 8 compares the results of the simulation, for various hole sizes and substrate thicknesses (in terms of the grid spacing), to the two models. As we can see, the area-weighted average model is almost perfectly accurate for d relatively large. In our substrates, we expect $d \approx 1\mu m$, while the other parameters are on the order of $100nm$, so this approximation should be perfectly adequate for our purposes.

Figure 7: An example run of our numerical simulation, showing the potential at all points in space, for the film held at $V = +1$, and the aluminum substrate at $V = -1$. The hole radius is set at $\frac{3}{7}$ of the maximum possible radius before holes overlap and $d = \frac{1}{2}$ times the distance between centers of holes. Equipotential surfaces are shown on a cross-section of three holes. Annotations are provided on the left half of the figure. Note that deep in the holes, the potential surfaces nearly match the level of their counterparts outside the holes.

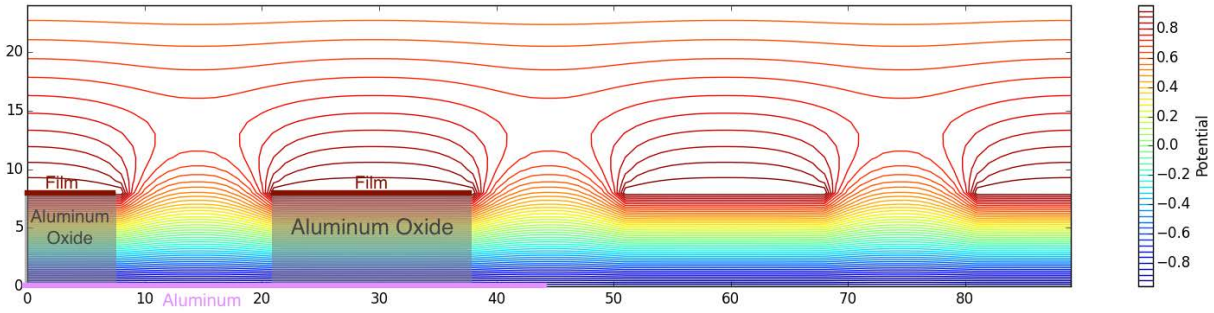

Figure 8: Comparison of simulated capacitances to the two approximations. The values given are the relative deviations of the two approximations from the simulated values: that is, the approximated capacitance minus the simulated capacitance, divided by the simulated capacitance. The units of the oxide thickness and hole size are given in units of one-half of the distance between the centers of adjacent holes.

Area-weighted Average Approximation, deviation from simulated capacitance

Hole Radius (in half hole spacings) \ Thickness (in half hole spacings)	0.25	0.5	1	2	4
0.14	1.8E-04	8.7E-05	4.3E-05	2.2E-05	1.3E-05
0.29	1.7E-03	8.7E-04	4.4E-04	2.2E-04	1.3E-04
0.43	6.6E-03	3.5E-03	1.8E-03	8.8E-04	5.1E-04
0.57	1.7E-02	9.3E-03	4.8E-03	2.4E-03	1.4E-03
0.71	3.9E-02	2.3E-02	1.2E-02	6.2E-03	3.6E-03
0.86	9.5E-02	5.9E-02	3.2E-02	1.6E-02	9.3E-03
1.00	4.8E-01	3.1E-01	1.7E-01	8.8E-02	5.0E-02

Neglected Holes Approximation, deviation from simulated capacitance

Hole Radius (in half hole spacings) \ Thickness (in half hole spacings)	0.25	0.5	1	2	4
0.14	-1.2E-03	-1.3E-03	-1.3E-03	-1.3E-03	-1.3E-03
0.29	-5.4E-03	-6.3E-03	-6.7E-03	-6.9E-03	-7.0E-03
0.43	-1.3E-02	-1.6E-02	-1.7E-02	-1.8E-02	-1.8E-02
0.57	-2.3E-02	-3.0E-02	-3.4E-02	-3.6E-02	-3.7E-02
0.71	-4.0E-02	-5.5E-02	-6.5E-02	-7.1E-02	-7.3E-02
0.86	-7.7E-02	-1.1E-01	-1.3E-01	-1.4E-01	-1.5E-01
1.00	-2.4E-01	-3.2E-01	-3.9E-01	-4.4E-01	-4.6E-01

7 Measurements of Total Capacitance per Unit Area

To measure film-substrate capacitances in films grown on Aluminum-AAO substrates, we first attempted direct measurement with an impedance bridge(a

General Radio 1620A). A 10.22 nm Ag film, with 1.03 nm Ge underlayer, was condensed onto an AAO substrate, and contacts were made using silver paint to both the film and to the aluminum substrate layer. The latter contact was made by scraping off a portion of oxide from the surface of the substrate. However, in ambient conditions, it was not possible to balance the bridge, suggesting changes in the capacitance with time as measurements were being taken. These changes are believed to be the result of fluctuations in environmental humidity: the introduction of water, with dielectric constant ≈ 80, into the pores of AAO can cause large changes in capacitance: in fact, this effect is used in commercial AAO-based humidity sensors.[7] Therefore, a vacuum chamber was retrofitted with an electrical feed-through and measurement stage to allow 3-terminal capacitance measurements to be made under vacuum, eliminating the effects of environmental moisture. Figure 9 shows the final setup, after some modifications discussed in section 8. Figure 10 shows the typical staging setup.

This allowed consistent measurements to be taken. To test the validity of the capacitance measurement scheme, eight 10.41 nm Ag/ 1.28 nm Ge films, of various areas, were condensed onto the same piece of AAO, and film-substrate capacitances were measured. The results are shown in Figure 11. Two films were excluded because contacts were accidentally made outside the bounds of the film, directly to AAO, causing anomalously large capacitance readings. Linear regression gives a capacitance per area of $19.7 \pm 0.4 \frac{pF}{mm^2}$, with a constant term of of $4.6 \pm 1.0 pF$, possibly due to stray capacitances in the system. The linearity of the graph shows that capacitance scales with film area, as expected: this implies that the film-substrate capacitance is in fact being measured.

Figure 9: Vacuum chamber for measuring capacitance. The pressure gauge was added when attempts were made to take measurements in inert gases. The aluminum foil provides electrical shielding of the feed-through. The thermometer is to monitor the stability of the temperature in the room: this was necessary for precise measurements; see section 8. Similarly, the copper coil and water bath were an attempt to stabilize the temperature in the chamber.

Figure 10: Staging platform for samples.

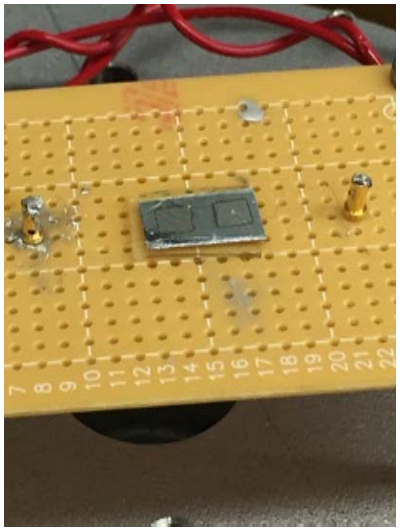

Figure 11: Film capacitance versus area in Ag / Ge NHC films. Linear regression gives a capacitance per area of $19.7 \pm 0.4 \frac{pF}{mm^2}$, with a y-intercept at $4.6 \pm 1.0 pF$. Error in area is due to stated precision of calipers used to measure film sizes: the actual precision may be lower due to human error in measurement; this may also explain the nonzero y-intercept

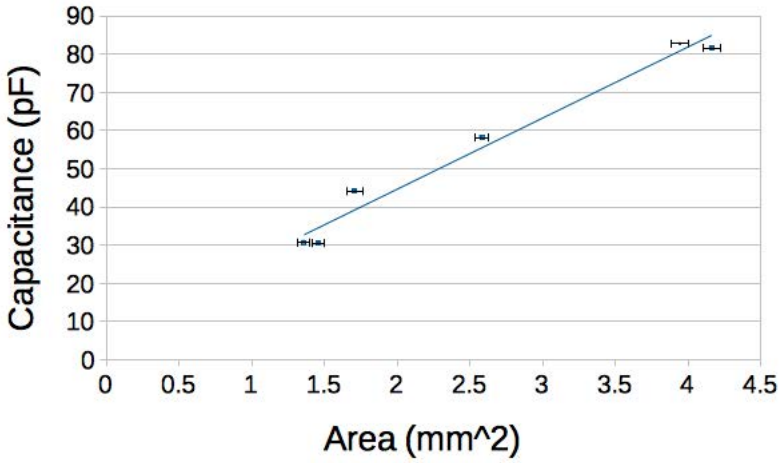

As a sanity check, if we assume zero pore area, this would give an oxide layer thickness of $4.57 \mu m$, which is of the correct order of magnitude: in actuality, we expect the dielectric constant to be greater, and the thickness smaller.

8 Attempts at Novel Methods for Measuring Film Thickness or Hole Area

Based on our formula for total capacitance:

$$C = \frac{A_{Al_2O_3}\epsilon_{Al_2O_3} + A_{hole}\epsilon_{hole}}{d} \tag{6}$$

We can see that, given reference values for dielectric constants and knowing the total area of the film and total capacitance (both of which are easily measured), we can achieve a measurement of all unknowns by either measuring d directly

or by measuring either $A_{Al_2O_3}$, A_{hole}, or the ratio between the two.

A scanning electron microscope measurement of either the surface or an broken edge of the substrate would be sufficient for all of these purposes. However, this is destructive to the sample, and is relatively costly and time-consuming compared to the other measurements. Attempts were made, therefore, to find an alternative method of measuring any of these values.

The method attempted was to saturate the substrate with an inert gas, and compare the capacitance to the capacitance in vacuum. By increasing the capacitance in the holes by a fixed proportion, one can theoretically ascertain the ratio between $A_{Al_2O_3}$ and A_{hole}. Nitrogen gas was tried first: [13] reports the dielectric constant of nitrogen at room temperature to be roughly $1 + .0005 * P$, where P is the pressure of the gas in atmospheres. Note that this leads to a very small change in total capacitance: if the holes takes up half the area of the film, this would be a change of roughly 0.004% in capacitance for one atmosphere of pressure. To measure changes of this magnitude, the output of the bridge was fed into a digital multimeter. Then, rather than re-balancing the bridge, the deflection of the balance could be compared to a known deflection made by changing the balance of the bridge.

Maintaining stable readings over time on this scale was difficult, even in vacuum. One possible explanation is the temperature dependence of the dielectric constant of aluminum oxide, which can vary by as much as 1% per 10 K temperature change.[14] Attempts were made to counteract this by frequently monitoring room temperature, and a bucket of water was heat-synced to the chamber to act as a heat bath.

Another issue was an anomalous spike in the capacitance that consistently occurred when gas was added to the chamber. This spike took several minutes to level off, which, due to the low signal-to-noise ratio and high variability of the

signal with time, was an obstacle to measurement. Adding smaller quantities of gas seemed to reduce the leveling time, so 100 millibar quantities of gas were used.

We were therefore able to obtain a consistent and non-transient change in capacitance as the gas was added. However, the magnitude of this change was slightly larger than what would be expected for any possible hole size: the maximum packing of circles in a hexagonal lattice covers 90.7% of the area, and the measured capacitance differences would correspond to an even larger fraction of the area being covered by holes: see Figure 12. As a control, helium gas, with dielectric constant an order of magnitude smaller than nitrogen, was used as a control. This showed roughly the same total change in capacitance as the nitrogen did, showing that the increase in capacitance due to adding the nitrogen gas was not in fact due to its increased dielectric constant. It is unknown what was in fact causing the increased capacitance with increasing gas concentration: it may have been a temperature effect, for example. However, we were not ultimately successful in devising a scheme to measure hole area through gas perfusion. Currently, liquid dielectrics such as methanol are being investigated as an alternative, but in this case, there is an issue of making sure that the pores are fully perfused, and that the volatility of the liquid does not affect the measurement.

9 Future Work

Attempts are ongoing to find an efficient and simple way of measuring the film thickness d. Also, we hope to correlate capacitance measurements with observed activation energies near the IST: some samples used in such activation energy measurements some years ago were found, but the films on them did not appear to be conductive at room temperature; this may be due to film oxidation from

Figure 12: Capacitance change versus Time, with inert gases added. Each spike shows response to the introduction of 100 mbar of gas. The film being tested in all experiments had initial capacitance of 72.3 pF, and area of $15.2mm^2$. The hole size of the substrate was 60 nm. Plots A and B are from experiments with nitrogen gas. Capacitance scales are given, relative to the final value of the capacitance. The values of p shown on each plot represent the initial levels that would correspond to different values of the porosity p, defined as $p = \frac{A_{hole}}{A_{total}}$. Both plots show a greater porosity than is possible for a packing of holes. Plot C shows repeated additions of five units of 100 mbar of nitrogen: note that the effects of each addition seem to be additive. Plot D shows the change in capacitance in response to the addition of helium ($\epsilon = 1.000006$ at 100 mbar). The magnitude of the effect is comparable to the effect in nitrogen ($\epsilon = 1.00005$ at 100 mbar), indicating that the dielectric effect of the gas in the pores was not the primary cause of the change in scale balance.

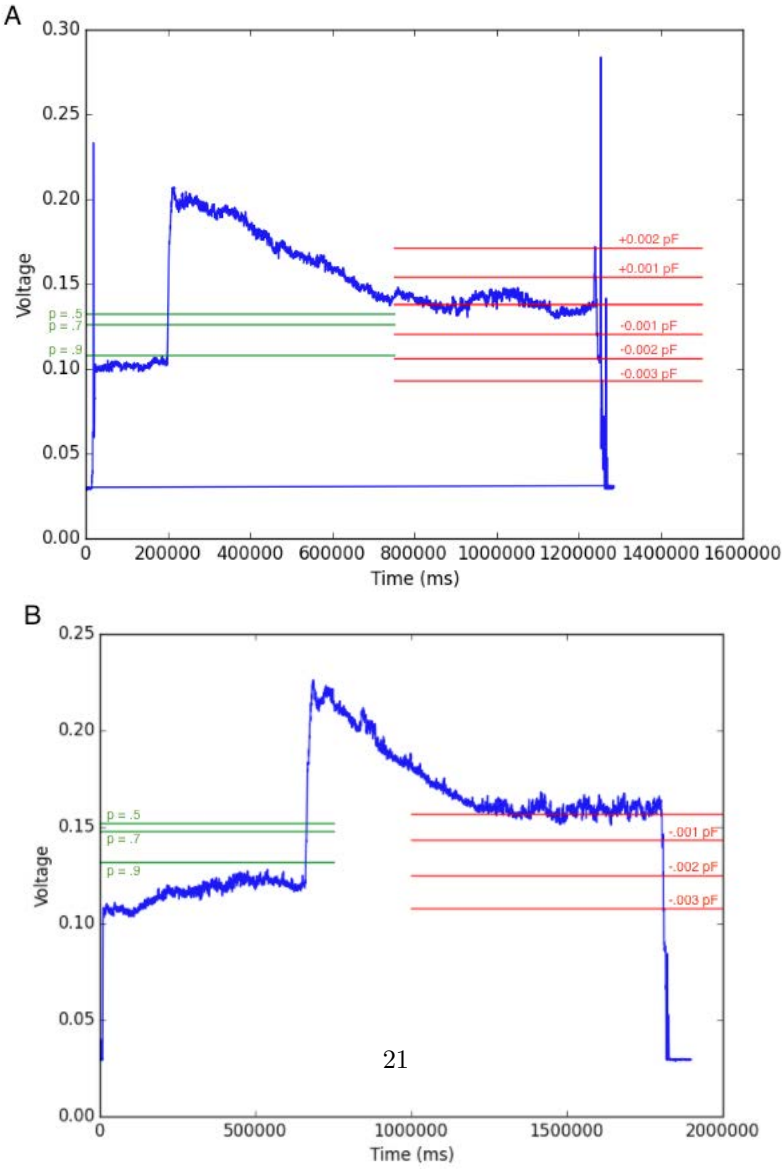

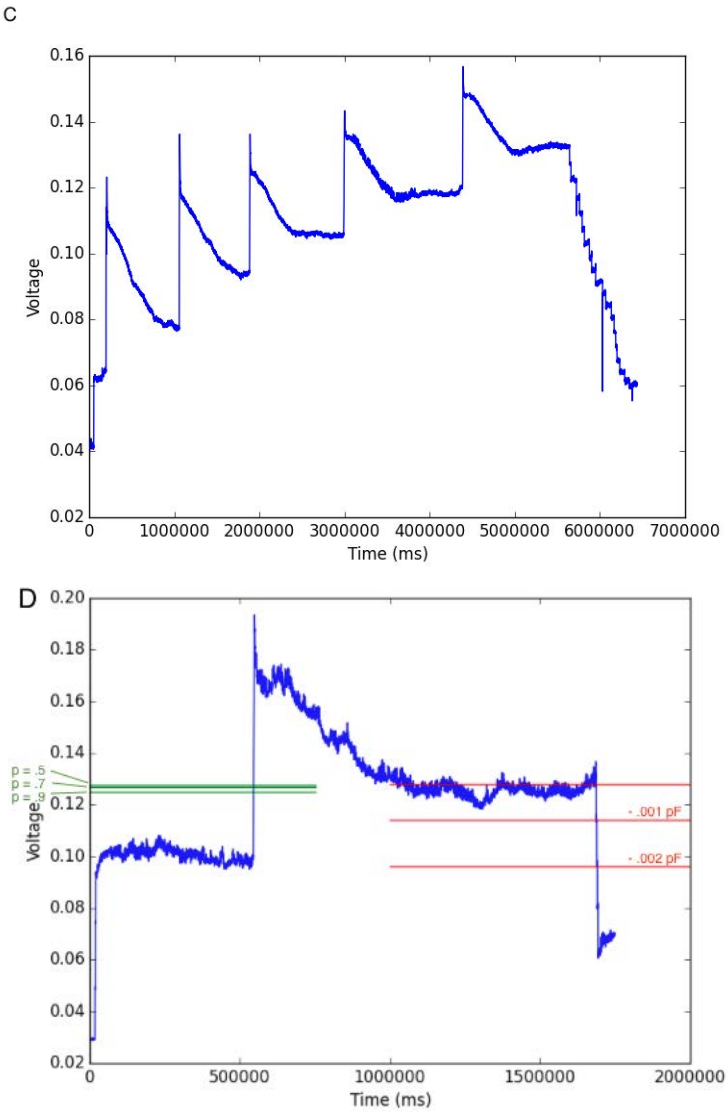
C
0.16
0.14
0.12
0.10
0.08
0.06
0.04
0.02
Voltage
0
1000000
2000000
3000000
4000000
5000000
6000000
7000000
Time (ms)
D
0.20
0.18
0.16
0.14
0.12
0.10
0.08
0.06
0.04
0.02
Voltage
p = .5
p = .7
p = .8
- .001 pF
- .002 pF
0
500000
1000000
1500000
2000000
Time (ms)

being stored in air.

10 Acknowledgements

I would like to thank Jimmy Joy and Xue Zhang for providing me with tremendous amounts of help in the lab.

11 Works Cited

[1] Stewart, M. D., Yin, A., Xu, J. M., & Valles, J. M. (2007). Superconducting pair correlations in an amorphous insulating nanohoneycomb film. Science, 318(5854), 1273-1275.

[2] Hollen, S. M., Nguyen, H. Q., Rudisaile, E., Stewart Jr, M. D., Shainline, J., Xu, J. M., & Valles Jr, J. M. (2011). Cooper-pair insulator phase in superconducting amorphous Bi films induced by nanometer-scale thickness variations. Physical Review B, 84(6), 064528.

[3] Stern, A. (1994). Quantum Hall fluid of vortices in a two-dimensional array of Josephson junctions. Physical Review B, 50(14), 10092.

[4] Kopeć, T. K., & José, J. V. (2001). Capacitance-matrix and geometrical effects on the ground-state properties of quantum Josephson-junction arrays. Physical Review B, 63(6), 064504.

[5] Delsing, P., Chen, C. D., Haviland, D. B., Harada, Y., & Claeson, T. (1994). Charge solitons and quantum fluctuations in two-dimensional arrays of small Josephson junctions. Physical Review B, 50(6), 3959.

[6] Astrakharchik, E. G., & Adkins, C. J. (1998). Superconductivity enhancement in screened ultrathin metal films. Journal of Physics: Condensed Matter, 10(21), 4509.

[7] Kim, Y., Jung, B., Lee, H., Kim, H., Lee, K., & Park, H. (2009). Capacitive humidity sensor design based on anodic aluminum oxide. Sensors and Actuators B: Chemical, 141(2), 441-446.

[8] Tighe, T. S., Tuominen, M. T., Hergenrother, J. M., & Tinkham, M. (1993). Measurements of charge soliton motion in two-dimensional arrays of ultrasmall Josephson junctions. Physical Review B, 47(2), 1145.

[9] Ortuño, M., Somoza, A. M., Vinokur, V. M., & Baturina, T. I. (2015). Electronic transport in two-dimensional high dielectric constant nanosystems.

Scientific reports, 5.

[10] Hollen, S. H. (2013) Cooper Pair Localization in Thin Films near the Superconductor-Insulator Transition. (Doctoral dissertation). Brown University, Providence, RI.

[11] Thorp, J. S., Akhtaruzzaman, M., & Evans, D. (1990). The dielectric properties of alumina substrates for microelectronic packaging. Journal of materials science, 25(9), 4143-4149.

[12] Nagel, J. R. (2011). Solving the Generalized Poisson Equation Using the Finite-Difference Method (FDM). Department of Electrical and Computer Engineering University of Utah, Salt Lake City, Utah. Retrieved from http://www.ece.utah.edu/ ece6340 /LECTURES/Feb1/Nagel%202012 %20-%20Solving%20the%20Generalized%20Poisson %20Equation%20using%20FDM.pdf.

[13] Jensen, J. E., Stewart, R. G., Tuttle, W. A., & Brechna, H. (1980). Brookhaven National Laboratory Selected Cryogenic Data Notebook. Brookhaven National Laboratory.

[14] Antula, J. (1967). Temperature dependence of dielectric constant of Al2O3. Physics Letters A, 25(4), 308.

[15] Al'tshuler, B. L., Aronov, A. G., & Zyuzin, A. Y. (1984). Size effects in disordered conductors. Sov. Phys. JETP, 59(2), 415.